3-2012

The Response of Calcareous Nannofossil Communities to Environmental Variation During the late middle Eocene at Blake Nose, Western North Atlantic, ODP Leg 171B

Johnathon P. Kell
University of Nebraska-Lincoln, jkell@huskers.unl.edu

The Response of Calcareous Nannofossil Communities to Environmental Variation During the late middle Eocene at Blake Nose, Western North Atlantic, ODP Leg 171B

by

Johnathon P. Kell

A THESIS

Presented to the Faculty of

The Graduate College at the University of Nebraska

In Partial Fulfillment of Requirements

For the Degree of Master of Science

Major: Earth & Atmospheric Sciences

Under the Supervision of Professor David K. Watkins

Lincoln, Nebraska

March, 2012

The Response of Calcareous Nannofossil Communities to Environmental Variation During the late middle Eocene at Blake Nose, Western North Atlantic, ODP Leg 171B

Johnathon P. Kell, M.S.

University of Nebraska, 2012

Advisor: David K. Watkins

Ocean Drilling Program Leg 171B Hole 1051B penetrated a continuous sequence of upper middle Eocene pelagic sediment dominated by rich calcareous nannofossil assemblages. Samples were taken at 10 cm spacing from a 20.2 meter section of the upper middle Eocene. This interval of pelagic sediment had previously been interpreted to represent ~500ky. Our revised age model, using additional data, indicates this section represents ~842ky.

The Eocene Epoch was characterized by one of the most dramatic climatic transitions in the last 65 my, changing the greenhouse earth of the early Eocene to the icehouse world of early Oligocene. Here changes in calcareous nannofossils communities are observed in association with climatic variability that accompanied this transition.

The relative abundance of calcareous nannofossil species was determined by conducting a count of 456 individuals for each of 203 samples. These data were analyzed using richness, diversity, and CABFAC factor analysis. This latter method showed 88.5% of the variance within the data was accounted for within two factors. Factor 1 displays a strong correlation with Shannon Diversity. The character and structure of the calcareous nannofossil communities were examined using Shannon diversity, species richness, and evenness. Shannon Diversity is shown

to have statistically significant correlations to richness and evenness. Richness and evenness are negatively correlated; Richness increases slightly up-section while evenness decreases slightly.

The calcareous nannofossil species present in each sample were also examined for biostratigraphic significance. It was determined that the upper middle Eocene sediments studied here are within Calcareous Nannofossil Zone CP14b. The extinction of *Sphenolithus obtusus* is of potential biostratigraphic value. *Sphenolithus obtusus* shows peak abundance of 12% in the lower portion of the section examined, a rapid decline in population followed. Assuming a constant rate of sediment accumulation (24 m/my), it is estimated to have taken approximately 126ky for *S. obtusus* to reach peak abundance and ~84ky to fall to 1% abundance levels where it persisted for another 100ky.

INTRODUCTION

The Eocene Epoch was characterized by one of the most dramatic climatic transitions in the last 65 m.y., changing the greenhouse earth of the early Eocene to the icehouse world of the early Oligocene. The Early Eocene Climatic Optimum (EECO; 50-52 Ma) exhibited deep sea temperatures up to 12˚ C warmer than present day. Following the EECO there was about 17 my of cooling, during which temperatures dropped to about 4 to 5˚ C above present day temperatures by late Eocene (Zachos et al., 2001). This cooling was part of a transition that led to the initiation of large scale glaciation of Antarctica during the earliest Oligocene (Lear et al., 2008). This cooling was global in scale and also affected the Northern Hemisphere (Dupont-Nivet et al., 2007).

Changes in the calcareous nannofossil assemblages preserved in the upper middle Eocene pelagic sediments of the Western North Atlantic provide a record of some of the initial oscillations in temperature that signals the decline in sea surface temperatures that accompanied this global cooling. Sea surface temperature (SST) data and paleoproductivity data from ODP Leg 171B Hole 1051B, produced by Wade et al. (2000) through the use of stable isotopes, provides the opportunity to correlate changes in calcareous nannofossil assemblages to the climatic variability that immediately preceded the Eocene/Oligocene cooling.

REGIONAL SETTING

The Blake Plateau was named after the U.S. Coastal Survey ship *Blake*, whose captain and crew acquired the first depth sounding measurements of the area in 1881 (Pratt, 1971).

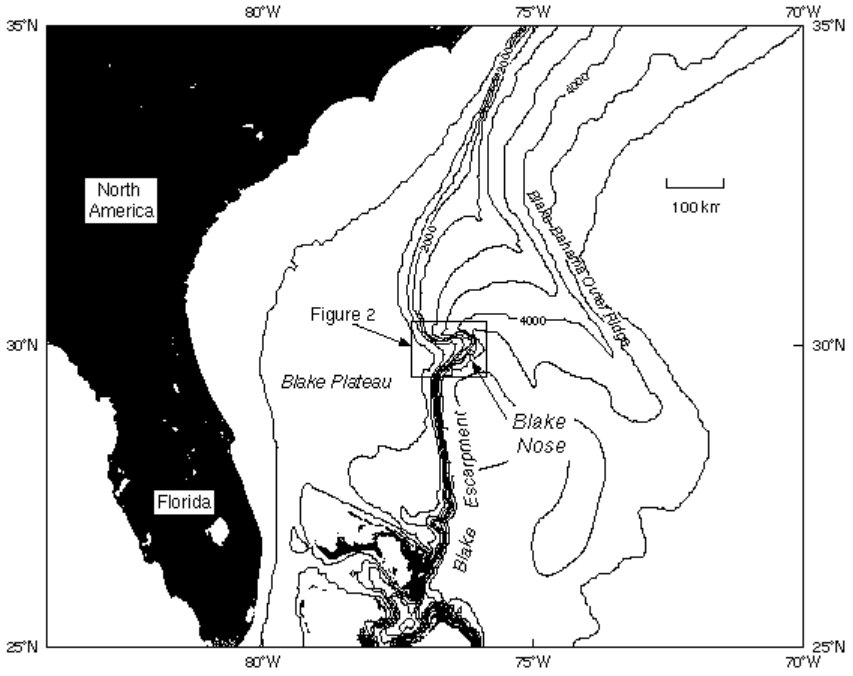

Figure 1: Location of Blake Nose in relation to the continent. (From Norris et al., 1998)

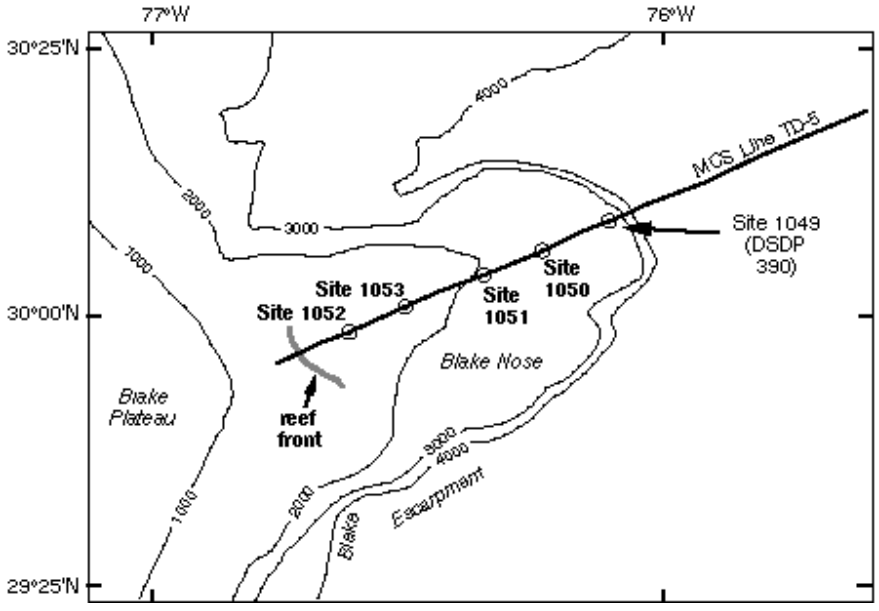

Figure 2: Enlarged from figure 1. Locations of drilling sites along the transect of Leg 171B. (From Norris et al., 1998)

Blake Nose is a prominent, eastward protruding, relatively gentle sloping ramp east of Florida that reaches a maximum depth of 2700 m. While the Blake Plateau is generally restricted to water depths of less than a kilometer the adjacent Blake

Escarpment (margin south of Blake Nose), is a nearly vertical wall that drops to depths greater than 4000 m into the Blake-Bahama Abyssal Plain (Pratt, 1971) (Figure 2).

Both Blake Plateau and Blake Nose are composed of thick Jurassic to lower Cretaceous reefal limestone sequences, which are overlain with less than 1 km of Upper Cretaceous and Cenozoic sedimentary rocks that are largely pelagic (Benson et al., 1978). Based on seismic evidence, Norris et al. (1998) concluded that Blake Nose is composed of a complex of buried reefs which served as a site for the seaward advance of fore-reef and pelagic deposits across a comparatively flat lying sequence of shallow water carbonates of Neocomian –Barremian age. Aptian-Cenomanian pelagic sediments laid down after this are disconformably overlain with Campanian to the lowest upper Eocene carbonate oozes that average. These pelagic sediments 400-600 m thick combined.

In 1997, ODP Leg 171B drilled five sites along a depth transect of Blake Nose. Samples of the upper middle Eocene section taken at ODP Hole 1051B, on Blake Nose in the western North Atlantic are the focus of this study. Sediments from these cores have undergone minimal diagenetic alteration. As a result of never having been deeply buried by younger sediment (Wade et al., 2001). Hole 1051B is located at 30°03.19`N, 76°21.47`W at a depth of 1980.6 meters below sea level. A total of 508.18 m of core was recovered spanning the upper Paleocene lowest to the upper Eocene. The thick section of upper middle Eocene, which consists of calcareous nannofossil ooze, shows moderately to well-preserved calcareous nannofossils. This section may indicate enhanced productivity in surface waters and/or favorable preservation conditions at the seafloor (Norris et al., 1998).

MATERIAL AND METHODS

The interval of sediment sampled in this study is composed of material from Hole 1051B, SubUnit IB (Figure 3). SubUnit IB is 61 m thick and consists of homogenous, clayey, pale yellow (tannish), nannofossil ooze with poorly defined bedding. It is overlain by a few meters of pelagic sediment containing manganese nodules that forms the current seafloor. A complete lithological description may be found in Norris et al., (1998).

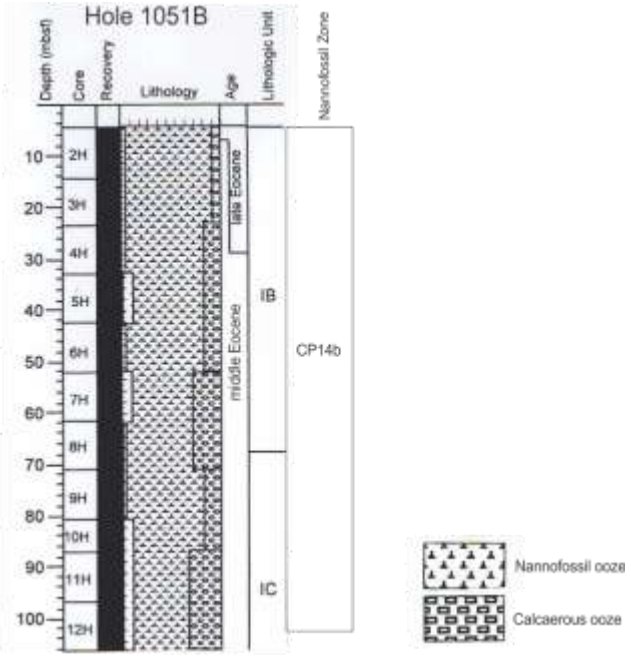

Figure 3. The lithology of the upper cores from Hole 1051B. All samples considered in this study fall within lithologic subunit IB (5.05 – 25.25 mbsf). Adapted from Norris et al. (1998).

Two hundred and three (203) samples from Hole 1051B were taken at 10 cm intervals through 20.2 m of core, between 1051B-2H1-25-26 cm to 1051B-4H1-115-116 cm (5.05 to 25.25 mbsf). This high resolution sampling covers a span of approximately 842,000 years (as explained below) during the latest middle Eocene and corresponds to part of calcareous nannofossil zone CP14b of Okada and Bukry (1980).

Raw sediment from each sample was used in the preparation of smear slides by the double slurry method, which has been demonstrated to provide reproducible data with 99% confidence (Watkins and Bergen, 2003). Each slide was prepared and mounted with Norland optical adhesive as described in Bown and Young (1998). Calcareous nannofossils present in each sample were examined with an Olympus BX51 light microscope (LM) using standard techniques with crossed polarized light and plane polarized light at 1250x magnification. Each sample was analyzed for species content and relative abundance. Relative abundances were logged as counts of 456 specimens. This count number provides abundance estimates that are within 5% of the actual proportion at the 95% confidence interval (Chang, 1967).

All data were analyzed using the PAST paleontological statistical program of Hammer et al. (2001) and/or OriginPro v. 7.5. The strengths of linear correlations between variables considered here are expressed using the Pearson correlation coefficient (r) as a measure of the correlation (linear dependence) between two variables and (p), the probability that the relationship is random. Correlations in this study with absolute values of correlation coefficients (r) greater than or equal to the absolute value of 0.30 and with (p) values less than 1.0×10^{-5} are considered significant. These values exceed those considered significant in a study with greater than 200 samples.

Diversity indices were used to assess the nature of the calcareous nannofossil assemblages observed over the considered interval. Species diversity has two components: richness and evenness. Species richness is the number of different species found within a given sample. Evenness refers to the numerical proportion of relative abundance between individual species within a sample. Values for evenness range from 0

to 1, where less variation between the populations of different species is equal to greater evenness. The Shannon diversity index is a measurement that employs both richness and evenness to produce an overall assessment of diversity and is also a measure of environmental stability (Sanders, 1968). Generally the values of the Shannon diversity index range from 1.5 (indicating low species richness and evenness) to 3.5 (high species evenness and richness).

The study interval was initially estimated to span approximately 500,000 years of late middle Eocene (Wade et al., 2001). A new age model was constructed for this study using data points higher in the core. These data (Table 1) were closer to and within the actual examined section, unlike those previously used. This age model for Hole 1051B was constructed using the magnetostratigraphy of the Shipboard Scientific Party of Leg 171B (Norris et al., 1998) and the geochronology of Berggren et al. (1995). As the sediments considered are not marked by any change in lithology or physical characteristics, the sedimentation rates between tie points are assumed to be constant and a regression line was extrapolated to the top of the studied section (Figure 4). The studied section between 5.05 to 25.25 mbsf is here calculated to represent approximately 842ky. Given this calculation, the 10 cm spacing of samples equates to about 4.2ky between samples. Ages for individual samples were determined using the equation of the regression line, and are listed in Appendix 1.

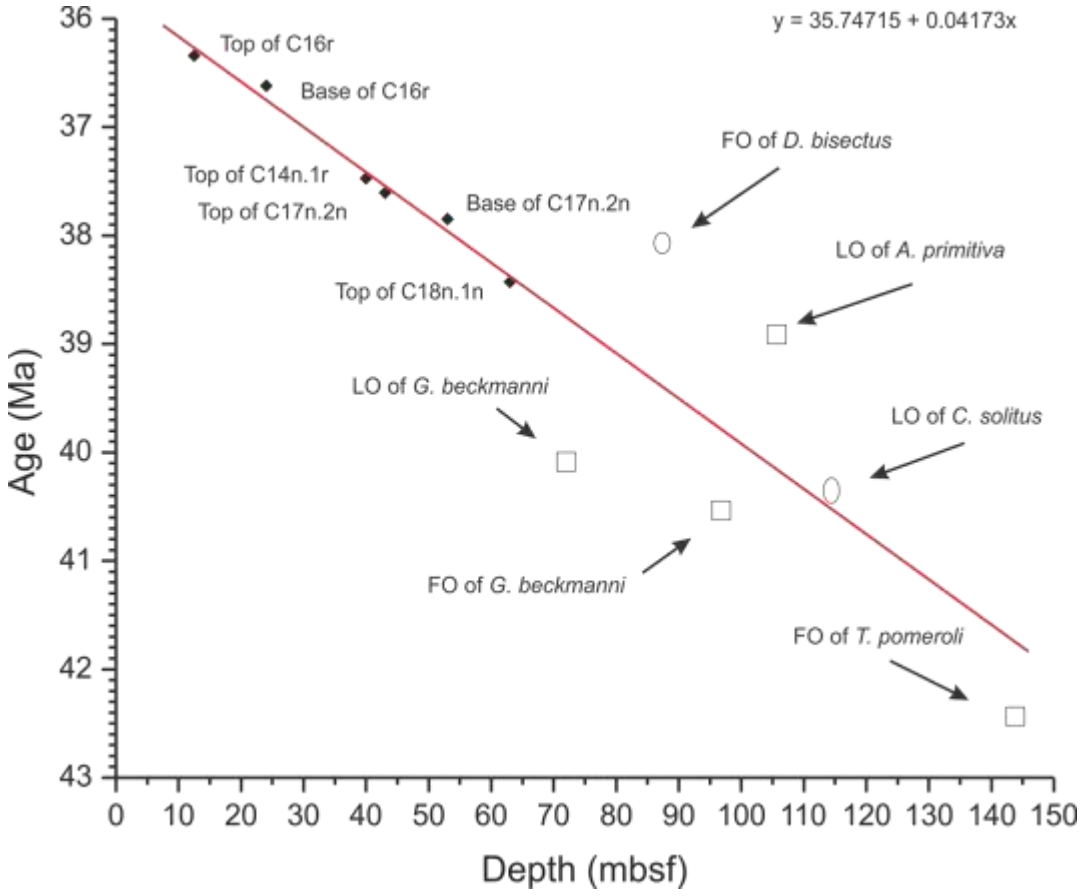

Figure 4. Age model constructed using the Shipboard magnetostratigraphy at Hole 1051B (Norris et al. 1998) and the age model from Berggren et al. (1995). Biostratigraphic age datums are from Wade et al. (2001). The formula for the regression line is displayed in the upper right, with the x coefficient indicating a sediment accumulation rate of approximately 24m/my. FO, first occurrence; LO, last occurrence. Squares, foraminifera datum; Ovoids, calcareous nannofossil datums.

Wade et al. (2000) produced a record of stable isotopes covering the interval in this study using planktonic and benthic foraminifera tests. Because we are concerned with the surface waters that calcareous nannofossils inhabited, the isotopic values used here are those of the planktonic foraminifera species. Interpretations of paleoceanographic SST's are made using $\delta^{18}O$ values. Changes in SST are calculated assuming no change in salinity and ice volume for late middle Eocene. Using the $\delta^{18}O$

temperature relationship, a $\delta^{18}O$ increase of 0.22‰ is equivalent to a 1 °C (1.8 °F) cooling (Visser et al., 2003). The general productivity of surface waters are interpreted using stable carbon isotopes, with higher values of $\delta^{13}C$ indicating increased productivity. As productivity increases in the surface waters $\delta^{13}C$ increases due to the preferential uptake of C^{12} by the planktonic community.

RESULTS

Census counts yielded forty-nine species within the 203 sampled assemblages of upper Middle Eocene calcareous nannofossils. These counts, assemblage statistics, and factor loadings for each sample are tabulated in Appendix Table 2.

Biostratigraphy

There is ambiguity in the calcareous nannofossil zonation assignments for the section under study in the initial reports of Site 1051 (Norris et al., 1998). The text discussion in Norris et al. (1998, p. 189) states that the first core recovered in Hole 1051B is placed within calcareous nannofossil zone CP15a based on the occurrence of *Chiasmolithus oamaruensis*, whereas their Figure 24 indicates that CP15a extends downwards to approximately 19 mbsf. In order to clarify this relationship, a detailed biostratigraphic evaluation of the section was performed.

The boundary between calcareous nannofossil subzones CP14b and CP15a is identified by the last occurrence (LO) of *Chiasmolithus grandis* or the first occurrence (FO) of *Chiasmolithus oamaruensis* (Perch-Nielsen, 1985). The genus *Chiasmolithus* is generally not common in tropical to temperate assemblages (e.g., Perch-Nielsen, 1985),

making identification of this subzonal boundary difficult in low latitudes. Examination of the assemblages from the studied section reveals rare specimens of *C. grandis* occurring sporadically throughout the studied section. This implies that the entire studied section (Sample 1051B-2H-1, 25 cm through 1051B-4H-1, 126 cm) lies within Subzone CP14b. A single specimen of *Chiasmolithus oamaruensis* was identified from Sample 1051B-3H-6, 35-36 cm. This species is known to occur in the core (1051B-1H) that overlies the studied interval. While the presence of this specimen might imply a CP15a assignment, the appearance of the single specimen in Core 1051B-3H is probably due to downhole contamination.

The LO of the marker species *Discoaster bifax* marks the boundary between CP14a and CP14b. An alternate marker is the LO of *Chiasmolithus solitus*. Both were absent in the studied interval, indicating that this part of the section is above the extinction level for *D. bifax* and *C. solitus*. This was expected, as the CP14a/CP14b boundary was originally placed at about 100 mbsf (Norris et al., 1998), approximately 75 m below the studied section. Therefore, the sediments within the studied interval (5.05 – 25.25 mbsf) are within the uppermost middle Eocene CP14b. This is in agreement with the foraminiferal zone data (P14) reported for these sediments in Norris et al. (1998).

The extinction of *Sphenolithus obtusus* and *Reticulofenestra dictyoda* are of biostratigraphic interest in this section. The percent abundance of *S. obtusus* shows an abundance peak of 12% in the lower portion of the section examined, followed by a rapid decline in population between 22 to 20 mbsf, with rare specimens persisting for several more meters at about 1% of the abundance. Assuming a constant rate of sediment accumulation (24 m/m.y.), it is then estimated to have taken approximately 126ky for *S.*

obtusus to reach peak abundance and about 84ky to fall to 1% abundance levels where it persisted for another 100ky. *Reticulofenestra dictyoda* exhibits a similar pattern. While *R. dictyoda* does not exhibit the same rapid rise in abundance as *S. obtusus*, it does experience a decline over the same span of time, 84ky. Perch-Nielsen (1985) indicates an extinction at the top of calcareous nannofossil zone CP14a; however, *R. dictyoda* persists well into CP14b at Blake Nose in significant abundances (>10%) until approximately 21mbsf and then in rare abundances (>2%) throughout the remainder of the examined section.

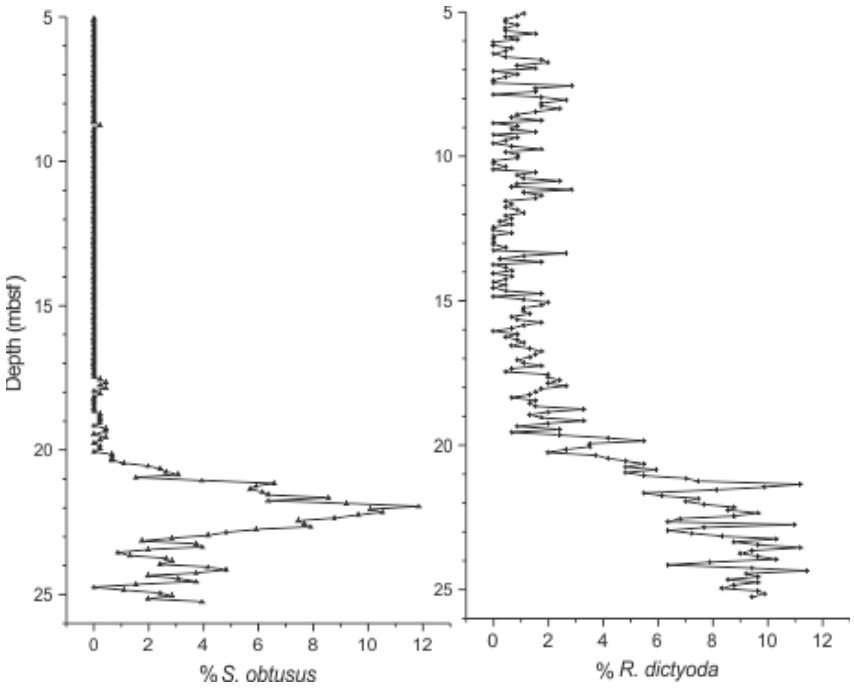

Figure 5. Percent abundances of *Sphenolithus obtusus* and *Reticulofenestra dictyoda* are shown. These two species also account for the two significant loadings of factor 2.

Perch-Nielsen (1985) notes that *Sphenolithus furcatolithoides* has its LO near the base of CP14b. According to Bukry (1971) *S. furcatolithoides* can be found in association with *Sphenolithus obtusus* near the base of *S. obtusus* (CP14a –CP15a, in Perch-Nielsen,

1985). In the studied interval S. *furcatolithoides* was noted to co-occur with *S. obtusus* more than 75 meters above the reported CP14a/CP14b boundary (Figure 3), suggesting that *S. furcatolithoides* persisted in rare abundance well into CP14b.

Assemblage Data

Sample assemblage richness ranged between 25 to 39 species, with an average of 32. The values for evenness range between 0.57 and 0.8 with an average value of 0.69. Values of the Shannon Diversity indices are between 2.85 and 3.35 and average 3.1. Figure 6 shows species richness and evenness compared with Shannon diversity using a 5 point moving average. The correlation between species richness and Shannon Diversity is (r) = 0.7405 and (p) = 1.5×10^{-36}. The correlation between species evenness and Shannon Diversity is not as strong but still statistically significant: (r) = 0.31 and (p) = 5.3×10^{-6}. There is a strong negative correlation between richness and evenness: (r) = -0.4 and (p) = 2.6×10^{-9}.

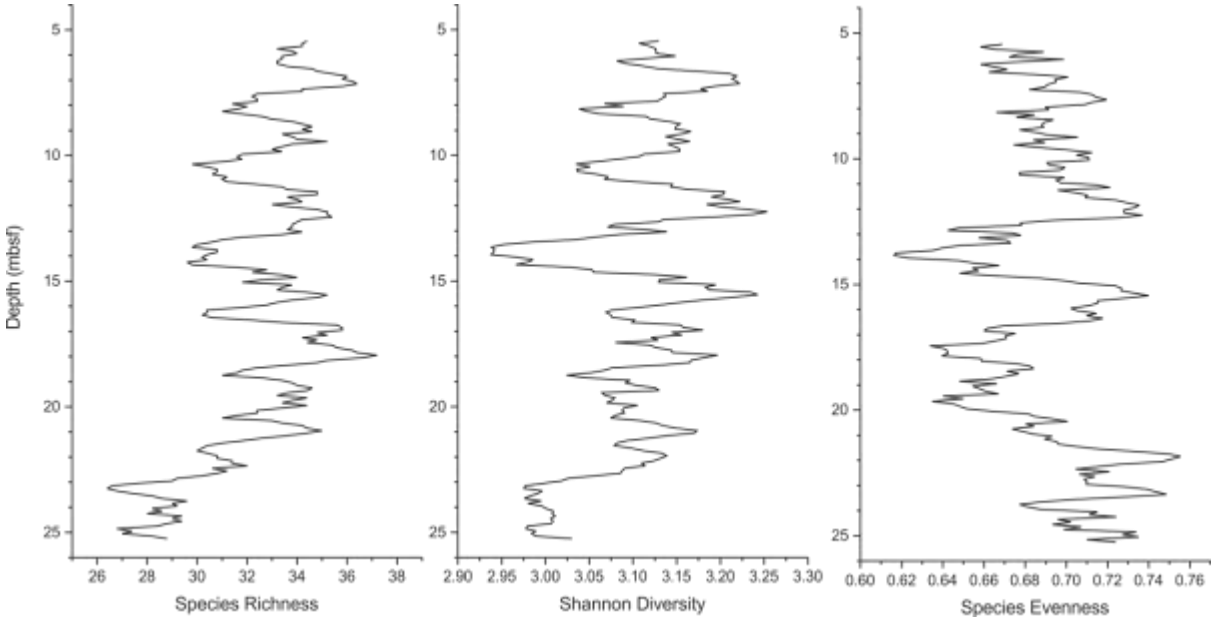

Figure 6. Species richness, Shannon Diversity, and species evenness shown using a 5 point moving average.

Where there are variations in the modulation of the evenness it is a function of the fluctuations in the abundance of a few select species, although the species responsible vary through the interval. *Cyclicargolithus floridans* is the most abundant taxon, on average, in the studied sections with abundances as high as 20%. There is a robust negative correlation ($r = -0.38$; $p = 1.4 \times 10^{-8}$) between evenness and the percent abundance of *C. floridans*. The largest declines in evenness, located at approximately 20, 18, and 14 mbsf, correspond to large dominance peaks of *C. floridans.* In the bottom 5 m of the interval, changes in the abundance of *S. obtusus* and *R. dictyoda* exert the greatest influence on evenness. Interestingly, as *S. obtusus* has its peak in abundance around 22 mbsf, all other species that had been previously dominant significantly declined over a period of about 42,000 years causing the maximum peak in evenness. *Cyclicargolithus floridans*, *Dictyococcites bisectus,* and *Coccolithus pelagicus* are the dominate taxa between approximately 20 – 15 mbsf. *Pemma papillata* displays a rise in abundance from about 15 – 12 mbsf that contributes to the largest decline in evenness. Given the calculated sediment accumulation rate, this decline is estimated to have occurred over an interval of approximately 125ky. The remainder of the interval shows a general trend of decreasing evenness, although with fluctuations.

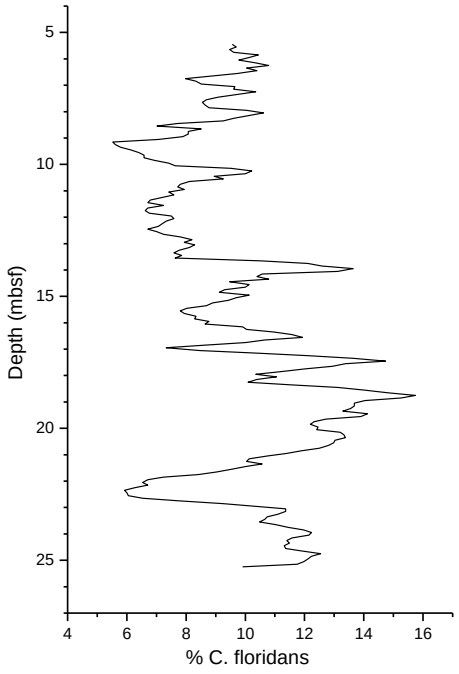

Figure 7. The abundance of *Cyclicargolithus floridans* shown as a 5 point moving average.

Quantitative Statistics

Q-Mode CABFAC factor analysis (Imbrie and Kipp, 1971; Klovan and Imbrie, 1971) showed two principal components with eigenvalues that account for 88.5% of the total variance. Factor 1 accounts for 84.6% of the variance with four significant positive loadings: *Coccolithus pelagicus*, (3.2), *Reticulofenestra scrippsae*,(2.8), *Discoaster saipanensis*,(2.7), and *Reticulofenestra wadeae*, (2.0) There is a positive overall trend (Figure 8) with the loading of factor 1 increasing from the base to the top of the considered interval. Factor one showed a high degree of correlation with Shannon diversity ($r = 0.42$; $p= 4.95 \times 10^{-10}$).

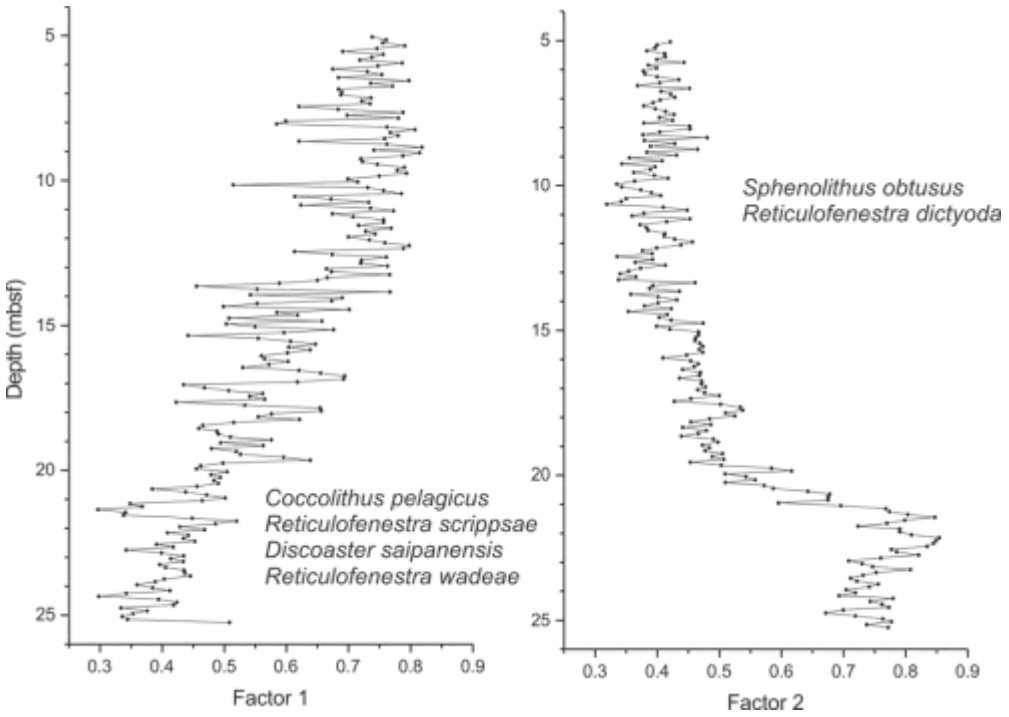

Figure 8. The distribution of loadings over the interval. Factor 1 is shown at left, factor 2 at right. The species responsible for the loadings in each factor are included.

Factor 2 accounts for 3.9% of the variance with two significant positive loadings: *Reticulofenestra dictyoda*, (4.8) and *Sphenolithus obtusus*, (3.3) (Figures 5 & 8). The loadings increase between the base and about 22 mbsf. There is rapid decrease in the loadings from approximately 21 to 20 mbsf with values decreasing from 0.85 to 0.45, respectively. The remainder of the interval displays a gradual, continued reduction in the loading values of factor 2 until about 10 mbsf. Continuing up through the section there is a slight increase in the overall values of about 0.1, until around 7 mbsf at which point the loading values continue to gradually diminish towards the top of the section.

Stable Isotopes

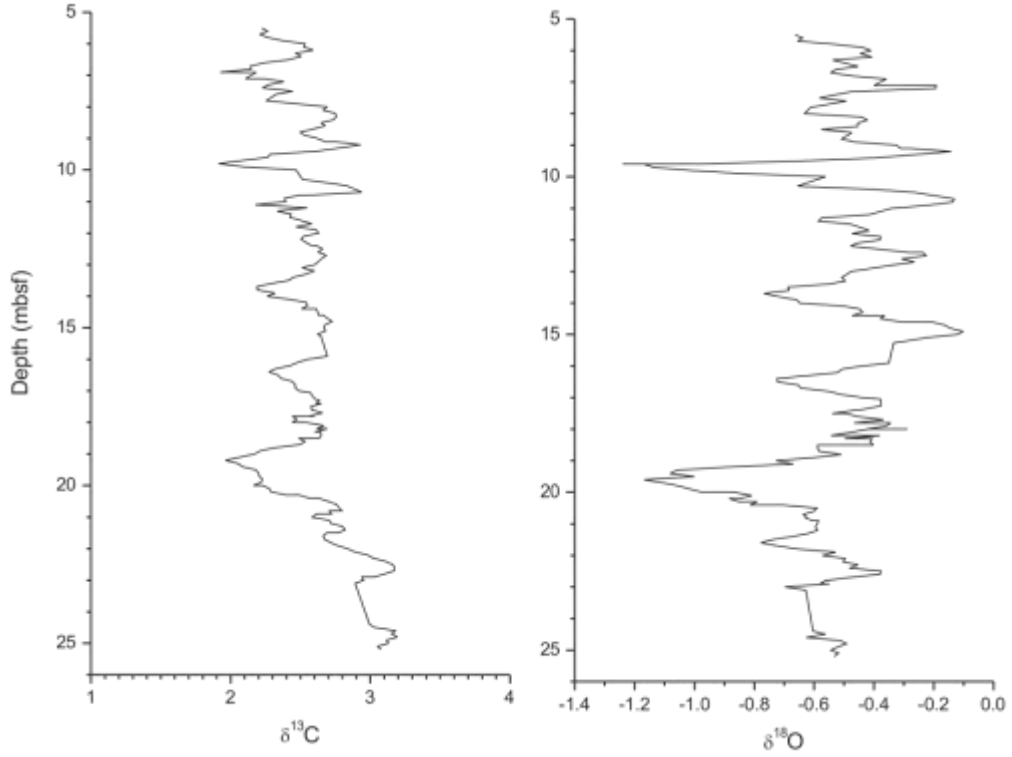

Figure 9. The distribution of $\delta^{13}C$ and $\delta^{18}O$ over the considered interval (5.05m -25.25m) shown as a 5 point moving average. Adapted from Wade et al. (2000).

The interval from 25.3 to 19 mbsf is characterized by a gradual and relatively steady decrease in carbon isotope values (from about 3.0 to 2.0 $\delta^{13}C$) and a decrease in oxygen isotope values (from approximately -0.4 to -1.2 $\delta^{18}O$). The carbon isotope record suggests a reduction in the primary production in the surface waters and a resultant decrease in the net export of organic matter to deeper water masses (Figure 9). The oxygen isotope record for this interval implies a warming of nearly 3°C, assuming no ice volume effects. This trend culminates in a prominent peak in both carbon and oxygen stable isotopes at approximately 19 mbsf. The isotopic values at this point suggest a significant decrease in productivity and that an increase in surface water temperature

occurred at this time. Thermal stratification of the water column would result in decreased mixing, leading to a decrease in the upwelled delivery of nutrients to surface waters.

The upper 10 meters does display several rapid fluctuations. Wade (2001) proposed cycles at ~ 1 meter spacing, which she interpreted as variations in the character of the water mass at Milankovitch frequencies (eccentricity and double peak precession) in the stable isotope data of benthic foraminifera.

DISCUSSION AND CONCLUSIONS

Construction of a revised age model for this section indicates a significantly longer span of time (842ky) than was previously reported. Biostratigraphic examination of the study section from Hole 1051B indicates that the entire section is within calcareous nannofossil Subzone CP14b of late middle Eocene age. The extinction level of *Sphenolithus obtusus* has been documented (Figure 5) within CP14b and offers an additional biostratigraphic indicator that may be useful over a wider geographic range. This species exhibited an abundance peak (comprising up to 12% of the total nannofossil assemblage), followed by a decline (<184ky) that culminated in its extinction at this location.

While both richness and evenness are shown to have positive correlations with Shannon diversity, richness and evenness correlate negatively with one another. From 25.3 to about 21 mbsf, richness generally increases (from a low of 25 to a high of 35) while evenness generally decreases. During this interval (from the 25 to 19 mbsf) $\delta^{18}O$

and $\delta^{13}C$ suggest a warming trend and reduction in surface water productivity, respectively (Figure 7). Richness has a relatively smaller range of fluctuation (~ 30 to 37) for the remainder of the section. Evenness varies widely (0.62 to 0.75) in the middle of the section, but varies less (0.66 to 0.72) near the top of the section. The reduction in variance of both richness and eveness in the upper 15 m of the section suggests increasing environmental stability. Significant short-term perturbations in the nannofossil assemblage structure, as indicated by abrupt declines in evenness located at approximately 20, 18, and 14 mbsf, correspond to large dominance peaks of *C. floridans*, indicating episodes of surface water disruption during the interval of general environmental stability. It's possible that the causes of these disruptions could be related to a variety of variables such as temperature or nutrient availability.

Q-Mode CABFAC factor analysis of the abundance data indicates that two principal components account for 88.5% of the total variance in the assemblage (Figure 8). Factor 1, which explains the vast majority of the variance (84.7%) in the assemblage census data, has a significant positive correlation with the Shannon diversity values ($r = 0.42$; $p = 4.9 \times 10^{-10}$). Factor 2 accounts for 3.9% of the variance in the cores. Two taxa have significant loadings on Factor 2.

The significant positive correlation between Factor 1 and Shannon diversity suggests that the changes in the assemblages, reflected by the gradual increase in CABFAC loadings with time, were accompanied by an increase in environmental stability in the surface waters. As the environment was stabilizing, $\delta^{13}C$ values became less positive. This is most prominent in the earlier portion of the succession, as represented by the core interval from 19-25.3 mbsf, suggesting a reduction in the action

of the biological pump. This decrease in carbon isotope values suggests that the surface waters became more oligotrophic with time. From this one might infer that the calcareous nannofossil community responded to increasing oligotrophy by an initial increase in species richness and a corresponding decrease in evenness, followed by increasing stability of the community, as indicate by decreasing variability of the diversity indices.

Sphenolithus obtusus increases to an abundance maximum (acme) at about 22 mbsf, and then exhibits a rapid decline towards extinction. *Reticulofenestra dictyoda* exhibits a similar rapid decrease in abundance at approximately the same depth. This ~84ky crash in abundance may be the result of the increase in SST's as represented in the $\delta^{18}O$ values, as well as the corresponding decline in primary production as evidenced in the decreasing $\delta^{13}C$ values over the same interval (Figure 9).

R. dictyoda was thought to go extinct at CP14a (Perch-Nielsen, 1985); however, at this location it persists in significant abundances until approximately 21mbsf and then at rare abundances throughout the remainder of the examined section, indicating that the total range of *R. dictyoda* extends beyond CP14a. Similarly, *S. obtusus* has previously been recognized as having a range of CP14a/b to CP15a (Perch-Nielsen, 1985); however, here *S. obtusus* goes extinct quite abruptly within CP14b

The calcareous nannofossil paleoecology coupled with the stable isotope data suggests that there was a significant change in the paleoenvironment of Site 1051 during the late middle Eocene. During the early part of this studied interval (represented by the basal 5 m of section) the surface water mass in the study area appears to have been warming by up to 3°C while simultaneously exhibiting progressively lower organic

productivity possibly due to thermal stratification of the water column. This environmental shift may have been partially responsible for the decreasing abundance and ultimate extinction of *Sphenolithus obtusus* and, to a lesser extent, *Reticulofenestra dictyoda*. This was followed by a period of more stable (less variable) surface water conditions.

Acknowledgements

I would like to thank my advisor, Dr. David K. Watkins, and my committee members Dr. Mary Anne Holmes and Dr. Ross Secord. Their comments and suggestions have greatly improved this manuscript. This research used samples provided by the Ocean Drilling Program (ODP). ODP is sponsored by the U.S. National Science Foundation (NSF) and participating countries under management of Joint Oceanographic Institutions (JOI), Inc. Funding for this research was provided by the University of Nebraska, Department of Earth and Atmospheric Sciences.

References

Benson, W.E., and Sheridan, R.E., et al., 1978. *Init. Repts. DSDP,*44: Washington (U.S. Govt. Printing Office).

Berggren, W A., Kent, D.V., Swisher III, C.C., and. Aubry, M.-P., 1995 A revised Cenozoic geochronology and chronostratigraphy, in Geochronology, Time Scales and Global Stratigraphic Correlation, Berggren, W. A. et al., (Eds.) Spec. Publ. SEPM Sediment. Geol., Vol. 54, pp.129–212.

Bown, P.R. and Young, J.R., 1998. Techniques. In: Calcareous Nannofossil Biostratigraphy, Kluwer Academic Publishers, United Kingdom at the University Press, Cambridge.

Bukry, D., 1971. Cenozoic Calcareous Nannofossils from the Pacific Ocean. Trans. San Diego Soc. Nat. Hist., 16:303-27.

Chang,Y.M., 1967. Accuracy of fossil percentage estimation. Journal of Paleontology 4, (1), 500-502.

Dupont-Nivet, G., Krijgsman, W., Langereis, C.G., Abels, H.A., Dai, S. & Fang, X., 2007. Tibetan plateau aridification linked to global cooling at the Eocene–Oligocene transition. Nature . 445, 635–638.

Hammer, Ø., Harper, D.A.T., and Ryan P.D., 2001. PAST: paleontological statistics software package for education and data analysis. Palaeontol. Electronica **4**. [Online.] http://palaeo-electronica.org/2001_1/past/issue1_01.htm.

Imbrie, J. and Kipp, N.G. , 1971. A new micropaleontological method for quantitative paleoclimatology: Application to a late Pleistocene Caribbean core. In: The Late

Cenozoic Glacial Ages, edited by K.K.Turekian, pp. 71-181, Yale Univ. Press, New Haven, CT.

Klovan, J.E. and Imbrie, J., 1971. An algorithm and FORTRAN-IV program for large scale Q-mode factoranalysis and calculation of factor scores. *Mathematical Geology*, 3:61-77.

Lear, C.H., Bailey, T.R., Pearson, P.N., Coxall, H.K., and Rosenthal, Y., 2008, Cooling and ice growth across the Eocene–Oligocene transition: *Geology*, 36: 251-254.

Norris, R.D., Kroon, D., and Klaus, A., 1998, Proceeding of the Ocean Drilling Program, Initial Results, Vol. 171B, Ocean Drilling Program, College Station, Texas, U.S.A.

Okada, H., and Bukry, D., 1980. Supplementary Modification and Introduction of Code Numbers to the Low-Latitude Coccolith Biostratigraphic Zonation. Marine Micropaleontology, 5, 321-325.

Perch-Nielsen, K., 1985. Cenozoic Calcareous Nannofossils. In: Bolli, H.M., Saunders, J.B., Perch-Nielsen, K. (Eds.) Plankton Stratigraphy. Cambridge University Press, Cambridge, pp. 427-554.

Pratt, R.M., 1971, Eastward Submarine Canyon and the Shaping of the Blake Nose, Geological Society of America Bulletin. 82, 2569-2576.

Sanders, H. L. 1968. Marine benthic diversity: a comparative study. Amer. Natur. 102, 243-282.

Visser, K., Thunell, R., Stott, L., 2003. Magnitude and timing of temperature in the Indo-Pacific warm pool during glaciation. Nature, Vol. 421, pp. 152– 155.

Wade, B.S., D. Kroon, and R.D. Norris. 2000. High-Resolution Stable Isotope Stratigraphy of the Late Middle Eocene at Site 1051, Blake Nose. Proceeding of the Ocean Drilling Program, Scientific Results, Vol. 171B, Ocean Drilling Program, College Station, Texas, U.S.A.

Wade, B.S., D. Kroon, and R.D. Norris. 2001. Orbitally forced climate change in late mid-Eocene time at Blake Nose (Leg 171B): evidence from stable isotopes in foraminifera. In: Kroon, D., Norris, R. D., and Klaus, A., (Eds.), Western North Atlantic Palaeogene and Cretaceous Palaeoceanography. Geological Society, London, Special Publication 183, pp. 273-292

Watkins, D. K., and Bergen, J. A., 2003, Late Albian adaptive radiation in the calcareous nannofossil genus *Eiffelithus.* Micropaleontology, Vol. 49, pp. 231-252.

Zachos, J., Pagani, M., Sloan, L., Thomas, E. & Billups, K. 2001. Trends, Rhythems, and Aberationsin Global Climate 65 Ma to Present. *Science,*Vol. 292, pp. 686–693.

Table 1.

Chron	**Age (Ma)**	**Depth (mbsf)**
C16r (top)	36.341	12.5
C16r (base)	36.618	24
C14n.1r (top)	37.473	40
C17n.2n (top)	37.604	43
C17n.2n (base)	37.848	53
C18n.1n (top)	38.426	63

Table 2

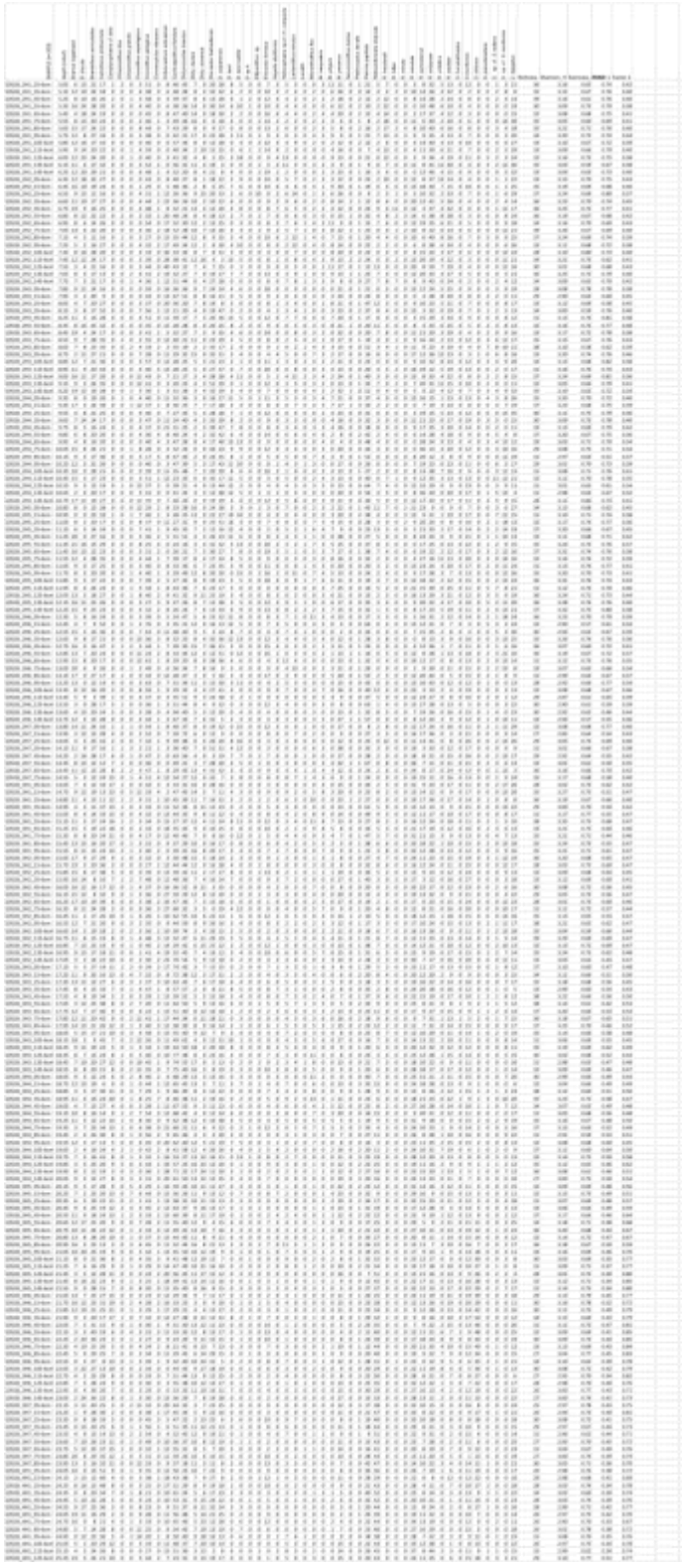

Plates and Plate Descriptions

Plate 1

Figure 1. *Braarudosphaera bigelowii* in cross polarized light (PO)

Figure 2. *Braarudosphaera discula* (PO)

Figure 3. *Bramletteius serraculoides* (PO)

Figure 4. *Campylosphaera* sp. cf. *C. dela* (PO)

Figure 5. *Chiasmolithus grandis* (PO)

Figure 6. *Chiasmolithus titus* (PO)

Figure 7.*Coccolithus eopelagicus* (PO)

Figure 8. *Coccolithus pelagicus* (PO)

Figure 9. *Coronocyclus nitescens* (PO).

Figure 10. *Calcidiscus protoannulus* (PO)

Figure 11. *Cribrocentrum reticulatum* (PO)

Figure 12. *Cyclicargolithus floridanus* (PO)

Figure 13. *Dictyococcites bisectus* (PO)

Figure 14. *Dictyococcites daviesii* (PO)

Figure 15. *Dictyococcites stavensis* (PO)

Figure 16. *Discoaster* sp. A. in plane polarized light (PPL).

Figure 17. *Discoaster barbadiensis* (PPL)

Figure 18. *Discoaster saipanensis* (PPL)

Figure 19. *Discoaster tanii* (PPL)

Figure 20. *Discoaster tanii nodifer* (PPL)

Plate 1


10.0 µm
1
5.0 µm
2
10.0 µm
3
10.0 µm
4
20.0 µm
5
10.0 µm
6
20.0 µm
7
10.0 µm
8
10.0 µm
9
10.0 µm
10
10.0 µm
11
5.0 µm
12
10.0 µm
13
10.0 µm
14
10.0 µm
15
10.0 µm
16
10.0 µm
17
10.0 µm
18
10.0 µm
19
10.0 µm
20

Plate 2

Figure 1. *Ellipsolithus* sp. (PO).

Figure 2. *Ericsonia formosa* (PO).

Figure 3. *Hayella situliformis* (PO).

Figure 4. *Helicosphaera* sp. cf. *H. compacta* (PO).

Figure 5. *Lanternlithus minutus* (PO).

Figure 6. *Loxolith* sp. indet (PO).

Figure 7. *Micrantholithus flos* (PO)

Figure 8. *Micrantholithus inaequalis* (PO)

Figure 9. *Micrantholithus pinguis* (PO)

Figure 10. *Micrantholithus procerus* (PO)

Figure 11. *Neococcolithes dubius* (PO)

Figure 12. *Pedinocyclus larvalis* (PO)

Figure 13. *Pemma papillatum* (PO)

Figure 14. *Reticulofenestra dictyoda* (PO)

Figure 15. *Reticulofenestra hesslandii* (PO).

Figure 16. *Reticulofenestra hillae* (PO)

Figure 17. *Reticulofenestra minuta* (PO)

Figure 18. *Reticulofenestra minutula* (PO)

Figure 19. *Reticulofenestra samodurovii* (PO)

Figure 20. *Reticulofenestra scrippsae* (PO)

Plate 2

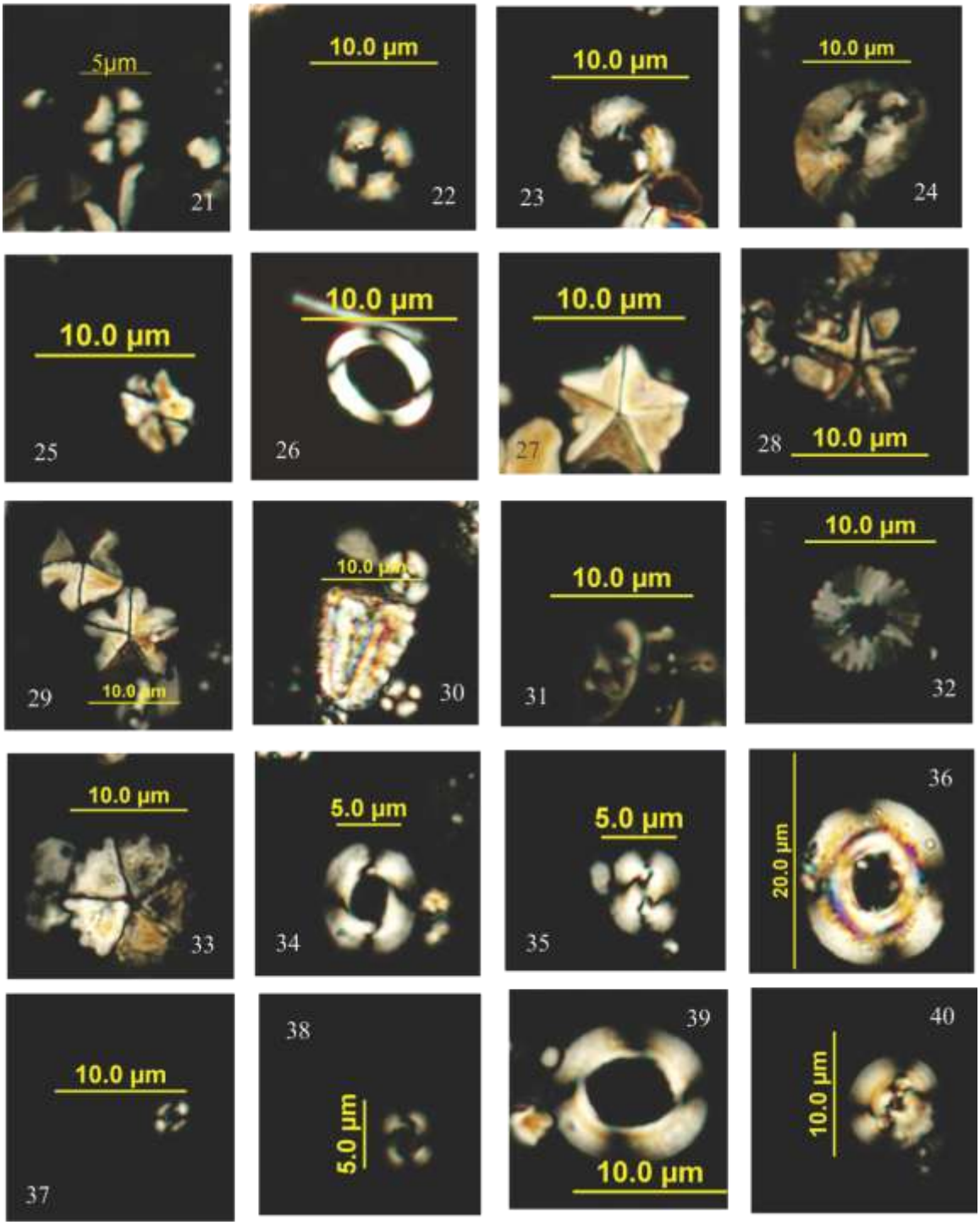
5µm
21
10.0 µm
22
10.0 µm
23
10.0 µm
24
10.0 µm
25
10.0 µm
26
10.0 µm
27
28
10.0 µm
29
10.0 µm
10.0 µm
30
10.0 µm
31
10.0 µm
32
10.0 µm
33
5.0 µm
34
5.0 µm
35
36
20.0 µm
10.0 µm
37
38
5.0 µm
39
10.0 µm
40
10.0 µm

Plate 3

Figure 1. *Reticulofenestra umbilica* (PO)

Figure 2. *Reticulofenestra wadeae* (PO)

Figures 3-4. *Sphenolithus furcatolithoides* (3 – PO; 4 - PPL)

Figures 5-6. *Sphenolithus moriformis* (5 – PO; 6 - PPL)

Figures 7-8. *Sphenolithus obtusus* (7 – PO; 8 - PPL)

Figures 9-10. *Sphenolilthus pseudoradians* (9 – PO; 10 - PPL)

Figures 11-12. *Sphenolithus radians* (11 – PO; 12 - PPL)

Figure 13. *Sphenolithus* sp. cf. *S. moriformis* (PO)

Figure 14. *Zygrhablithus bijugatus* (PO)

Plate 3

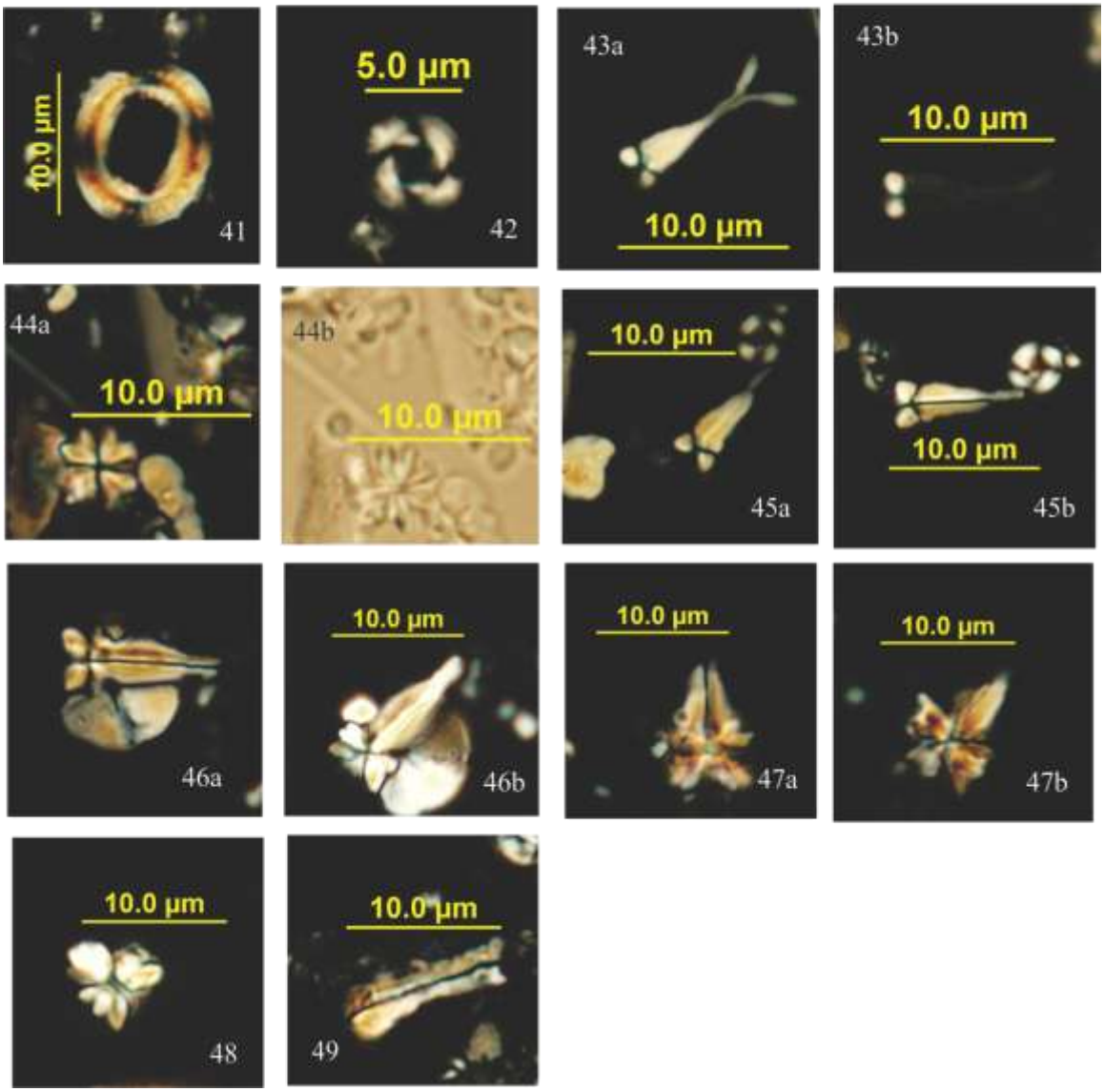
10.0 µm
41
5.0 µm
42
43a
10.0 µm
43b
10.0 µm
44a
10.0 µm
44b
10.0 µm
10.0 µm
45a
10.0 µm
45b
46a
10.0 µm
46b
10.0 µm
47a
10.0 µm
47b
10.0 µm
48
10.0 µm
49

Appendix 1

SAMPLE (n=203)	Depth (mbsf)	Age(Ma)
1051B_2H1_25-6cm	5.05	35.95759
1051B_2H1_35-6cm	5.15	35.96176
1051B_2H1_45-6cm	5.25	35.96593
1051B_2H1_55-6cm	5.35	35.9701
1051B_2H1_65-6cm	5.45	35.97427
1051B_2H1_75-6cm	5.55	35.97844
1051B_2H1_85-6cm	5.65	35.98261
1051B_2H1_95-6cm	5.75	35.98678
1051B_2H1_105-6cm	5.85	35.99095
1051B_2H1_115-6cm	5.95	35.99512
1051B_2H1_125-6cm	6.05	35.99929
1051B_2H1_135-6cm	6.15	36.00346
1051B_2H1_145-6cm	6.25	36.00763
1051B_2H2_05-6cm	6.35	36.0118
1051B_2H2_15-6cm	6.45	36.01597
1051B_2H2_25-6cm	6.55	36.02014
1051B_2H2_35-6cm	6.65	36.02431
1051B_2H2_45-6cm	6.75	36.02848
1051B_2H2_55-6cm	6.85	36.03265
1051B_2H2_65-6cm	6.95	36.03682
1051B_2H2_75-6cm	7.05	36.04099
1051B_2H2_85-6cm	7.15	36.04516
1051B_2H2_95-6cm	7.25	36.04933
1051B_2H2_105-6cm	7.35	36.0535
1051B_2H2_115-6cm	7.45	36.05767
1051B_2H2_125-6cm	7.55	36.06184
1051B_2H2_135-6cm	7.65	36.06601
1051B_2H2_145-6cm	7.75	36.07018
1051B_2H3_05-6cm	7.85	36.07435
1051B_2H3_15-6cm	7.95	36.07852
1051B_2H3_25-6cm	8.05	36.08269
1051B_2H3_35-6cm	8.15	36.08686
1051B_2H3_45-6cm	8.25	36.09103
1051B_2H3_55-6cm	8.35	36.0952
1051B_2H3_65-6cm	8.45	36.09937

1051B_2H3_75-6cm	8.55	36.10354
1051B_2H3_85-6cm	8.65	36.10771
1051B_2H3_95-6cm	8.75	36.11188
1051B_2H3_105-6cm	8.85	36.11605
1051B_2H3_115-6cm	8.95	36.12022
1051B_2H3_125-6cm	9.05	36.12439
1051B_2H3_135-6cm	9.15	36.12856
1051B_2H3_145-6cm	9.25	36.13273
1051B_2H4_05-6cm	9.35	36.1369
1051B_2H4_15-6cm	9.45	36.14107
1051B_2H4_25-6cm	9.55	36.14524
1051B_2H4_35-6cm	9.65	36.14941
1051B_2H4_45-6cm	9.75	36.15358
1051B_2H4_55-6cm	9.85	36.15775
1051B_2H4_65-6cm	9.95	36.16192
1051B_2H4_75-6cm	10.05	36.16609
1051B_2H4_85-6cm	10.15	36.17026
1051B_2H4_95-6cm	10.25	36.17443
1051B_2H4_105-6cm	10.35	36.1786
1051B_2H4_115-6cm	10.45	36.18277
1051B_2H4_125-6cm	10.55	36.18694
1051B_2H4_135-6cm	10.65	36.19111
1051B_2H4_145-6cm	10.75	36.19528
1051B_2H5_05-6cm	10.85	36.19945
1051B_2H5_15-6cm	10.95	36.20362
1051B_2H5_25-6cm	11.05	36.20779
1051B_2H5_35-6cm	11.15	36.21196
1051B_2H5_45-6cm	11.25	36.21613
1051B_2H5_55-6cm	11.35	36.2203
1051B_2H5_65-6cm	11.45	36.22447
1051B_2H5_75-6cm	11.55	36.22864
1051B_2H5_85-6cm	11.65	36.23281
1051B_2H5_95-6cm	11.75	36.23698
1051B_2H5_105-6cm	11.85	36.24115
1051B_2H5_115-6cm	11.95	36.24532
1051B_2H5_125-6cm	12.05	36.24949
1051B_2H5_135-6cm	12.15	36.25366
1051B_2H5_145-6cm	12.25	36.25783
1051B_2H6_05-6cm	12.35	36.262
1051B_2H6_15-6cm	12.45	36.26617
1051B_2H6_25-6cm	12.55	36.27034
1051B_2H6_35-6cm	12.65	36.27451
1051B_2H6_45-6cm	12.75	36.27868

1051B_2H6_55-6cm	12.85	36.28285
1051B_2H6_65-6cm	12.95	36.28702
1051B_2H6_75-6cm	13.05	36.29119
1051B_2H6_85-6cm	13.15	36.29536
1051B_2H6_95-6cm	13.25	36.29953
1051B_2H6_105-6cm	13.35	36.3037
1051B_2H6_115-6cm	13.45	36.30787
1051B_2H6_125-6cm	13.55	36.31204
1051B_2H6_135-6cm	13.65	36.31621
1051B_2H6_145-6cm	13.75	36.32038
1051B_2H7_05-6cm	13.85	36.32455
1051B_2H7_15-6cm	13.95	36.32872
1051B_2H7_25-6cm	14.05	36.33289
1051B_2H7_35-6cm	14.15	36.33706
1051B_2H7_45-6cm	14.25	36.34123
1051B_2H7_55-6cm	14.35	36.3454
1051B_2H7_65-6cm	14.45	36.34957
1051B_2H7_75-6cm	14.55	36.35374
1051B_3H1_05-6cm	14.65	36.35791
1051B_3H1_15-6cm	14.75	36.36208
1051B_3H1_25-6cm	14.85	36.36625
1051B_3H1_35-6cm	14.95	36.37042
1051B_3H1_45-6cm	15.05	36.37459
1051B_3H1_55-6cm	15.15	36.37876
1051B_3H1_65-6cm	15.25	36.38293
1051B_3H1_75-6cm	15.35	36.3871
1051B_3H1_85-6cm	15.45	36.39127
1051B_3H1_95-6cm	15.55	36.39544
1051B_3H2_05-6cm	15.65	36.39961
1051B_3H2_15-6cm	15.75	36.40378
1051B_3H2_25-6cm	15.85	36.40795
1051B_3H2_35-6cm	15.95	36.41212
1051B_3H2_45-6cm	16.05	36.41629
1051B_3H2_55-6cm	16.15	36.42046
1051B_3H2_65-6cm	16.25	36.42463
1051B_3H2_75-6cm	16.35	36.4288
1051B_3H2_85-6cm	16.45	36.43297
1051B_3H2_95-6cm	16.55	36.43714
1051B_3H2_105-6cm	16.65	36.44131
1051B_3H2_115-6cm	16.75	36.44548
1051B_3H2_125-6cm	16.85	36.44965
1051B_3H2_135-6cm	16.95	36.45382
1051B_3H2_145-6cm	17.05	36.45799

1051B_3H3_05-6cm	17.15	36.46216
1051B_3H3_15-6cm	17.25	36.46633
1051B_3H3_25-6cm	17.35	36.4705
1051B_3H3_35-6cm	17.45	36.47467
1051B_3H3_45-6cm	17.55	36.47884
1051B_3H3_55-6cm	17.65	36.48301
1051B_3H3_65-6cm	17.75	36.48718
1051B_3H3_75-6cm	17.85	36.49135
1051B_3H3_85-6cm	17.95	36.49552
1051B_3H3_95-6cm	18.05	36.49969
1051B_3H3_105-6cm	18.15	36.50386
1051B_3H3_115-6cm	18.25	36.50803
1051B_3H3_125-6cm	18.35	36.5122
1051B_3H3_135-6cm	18.45	36.51637
1051B_3H3_145-6cm	18.55	36.52054
1051B_3H4_05-6cm	18.65	36.52471
1051B_3H4_15-6cm	18.75	36.52888
1051B_3H4_25-6cm	18.85	36.53305
1051B_3H4_35-6cm	18.95	36.53722
1051B_3H4_45-6cm	19.05	36.54139
1051B_3H4_55-6cm	19.15	36.54556
1051B_3H4_65-6cm	19.25	36.54973
1051B_3H4_75-6cm	19.35	36.5539
1051B_3H4_85-6cm	19.45	36.55807
1051B_3H4_95-6cm	19.55	36.56224
1051B_3H4_105-6cm	19.65	36.56641
1051B_3H4_115-6cm	19.75	36.57058
1051B_3H4_125-6cm	19.85	36.57475
1051B_3H4_135-6cm	19.95	36.57892
1051B_3H4_145-6cm	20.05	36.58309
1051B_3H5_05-6cm	20.15	36.58726
1051B_3H5_15-6cm	20.25	36.59143
1051B_3H5_25-6cm	20.35	36.5956
1051B_3H5_35-6cm	20.45	36.59977
1051B_3H5_45-6cm	20.55	36.60394
1051B_3H5_55-6cm	20.65	36.60811
1051B_3H5_65-6cm	20.75	36.61228
1051B_3H5_75-6cm	20.85	36.61645
1051B_3H5_85-6cm	20.95	36.62062
1051B_3H5_95-6cm	21.05	36.62479
1051B_3H5_105-6cm	21.15	36.62896
1051B_3H5_115-6cm	21.25	36.63313
1051B_3H5_125-6cm	21.35	36.6373

1051B_3H5_135-6cm	21.45	36.64147
1051B_3H5_145-6cm	21.55	36.64564
1051B_3H6_05-6cm	21.65	36.64981
1051B_3H6_15-6cm	21.75	36.65398
1051B_3H6_25-6cm	21.85	36.65815
1051B_3H6_35-6cm	21.95	36.66232
1051B_3H6_45-6cm	22.05	36.66649
1051B_3H6_55-6cm	22.15	36.67066
1051B_3H6_65-6cm	22.25	36.67483
1051B_3H6_75-6cm	22.35	36.679
1051B_3H6_85-6cm	22.45	36.68317
1051B_3H6_95-6cm	22.55	36.68734
1051B_3H6_105-6cm	22.65	36.69151
1051B_3H6_115-6cm	22.75	36.69568
1051B_3H6_125-6cm	22.85	36.69985
1051B_3H6_135-6cm	22.95	36.70402
1051B_3H6_145-6cm	23.05	36.70819
1051B_3H7_05-6cm	23.15	36.71236
1051B_3H7_15-6cm	23.25	36.71653
1051B_3H7_25-6cm	23.35	36.7207
1051B_3H7_35-6cm	23.45	36.72487
1051B_3H7_45-6cm	23.55	36.72904
1051B_3H7_55-6cm	23.65	36.73321
1051B_3H7_65-6cm	23.75	36.73738
1051B_3H7_75-6cm	23.85	36.74155
1051B_3H7_85-6cm	23.95	36.74572
1051B_4H1_05-6cm	24.05	36.74989
1051B_4H1_15-6cm	24.15	36.75406
1051B_4H1_25-6cm	24.25	36.75823
1051B_4H1_35-6cm	24.35	36.7624
1051B_4H1_45-6cm	24.45	36.76657
1051B_4H1_55-6cm	24.55	36.77074
1051B_4H1_65-6cm	24.65	36.77491
1051B_4H1_75-6cm	24.75	36.77908
1051B_4H1_85-6cm	24.85	36.78325
1051B_4H1_95-6cm	24.95	36.78742
1051B_4H1_105-6cm	25.05	36.79159
1051B_4H1_115-6cm	25.15	36.79576
1051B_4H1_125-6cm	25.25	36.79993

Appendix 2

Calcareous Nannofossil Taxa Considered In This Study

Braarudosphaera bigelowii (Gran & Braarud, 1935) Deflandre, 1947

Braarudosphaera discula Bramlette & Riedel, 1954

Bramletteius serraculoides Gartner, 1969

Campylosphaera sp. cf. *C. dela* Hay & Mohler, 1967

Chiasmolithus grandis (Bramlette & Riedel, 1954) Radomski (1968)

Chiasmolithus titus Gartner, 1970

Coccolithus eopelagicus (Bramlette & Riedel, 1954) Bramlette & Sullivan, 1961

Coccolithus pelagicus (Wallich, 1877) Schiller, 1930

Coronocyclus nitescens (Kamptner, 1963) Bramlette & Wilcoxon, 1967

Calcidiscus protoannulus (Gartner, 1971) Loeblich & Tappan, 1978

Cribrocentrum reticulatum (Gartner & Smith, 1967) Perch-Nielsen, 1971

Cyclicargolithus floridanus (Hay et al., 1967) Bukry, 1971

Dictyococcites bisectus (Hay et al., 1966) Bukry and Percival, 1971

Dictyococcites daviesii Perch-Nielsen, 1971

Dictyococcites stavensis (Levin & Joerger, 1967) Varol, 1998

Discoaster sp. A

Discoaster barbadiensis Tan, 1927

Discoaster saipanensis Bramlette & Riedel, 1954

Discoaster tanii Bramlette & Riedel, 1954

Discoaster tanii nodifer Bramlette & Riedel, 1954

Ellipsolithus sp.

Ericsonia formosa Haq, 1971

Hayella situliformis Gartner, 1969

Helicosphaera sp. cf. *H. compacta* Bramlette & Wilcoxon, 1967

Lanternlithus minutus Stradner 1962

Loxolith sp. indet.

Micrantholithus flos (Deflandre, 1950) Deflandre in Deflandre & Fert, 1954

Micrantholithus inaequalis Martini 1961

Micrantholithus pinguis Bramlette & Sullivan, 1961

Micrantholithus procerus Bukry & Bramlette, 1969

Neococcolithes dubius (Deflandre in Deflandre & Fert, 1954) Black, 1967

Pedinocyclus larvalis (Bukry & Bramlette, 1969) Loeblich & Tappan, 1973

Pemma papillatum Martini, 1959

Reticulofenestra dictyoda (Deflandre in Deflandre & Fert, 1954) Stradner in Stradner & Edwards, 1968

Reticulofenestra hesslandii Roth, 1970

Reticulofenestra hillae Bukry & Percival, 1971

Reticulofenestra minuta Roth, 1970

Reticulofenestra minutula (Gartner, 1967) Haq & Berggren, 1978

Reticulofenestra samodurovii (Hay, Mohler & Wade, 1966) Roth, 1970

Reticulofenestra scrippsae (Bukry & Percival, 1971) Roth, 1973

Reticulofenestra umbilica (Levin, 1965) Martini & Ritzkowski, 1968

Reticulofenestra wadeae Bown, 2005

Sphenolithus furcatolithoides Locker, 1967

Sphenolithus moriformis (Brönnimann and Stradner, 1960) Bramlette and Wilcoxon, 1967

Sphenolithus obtusus Bukry, 1971

Sphenolilthus pseudoradians Bramlette and Wilcoxon, 1967

Sphenolithus radians Deflandre in Grasse, 1952

Sphenolithus sp. cf. *S. moriformis* (Brönnimann and Stradner, 1960) Bramlette and Wilcoxon, 1967

Zygrhablithus bijugatus (Deflandre in Deflandre & Fert, 1954) Deflandre, 1959